

001
002
003
004
005
006
007
008
009
010
011
012
013
014
015
016
017
018
019
020
021
022
023
024
025
026
027
028
029
030
031
032
033
034
035
036
037
038
039
040
041
042
043
044
045
046

ChimeraLM: A genomic language model that distinguishes true structural variants from artifacts in whole-genome amplification-based long-read sequencing

Yangyang Li^{1†}, Qingxiang Guo^{1†}, Rendong Yang^{1,2*}

¹Department of Urology, Northwestern University Feinberg School of Medicine, 303 E Superior St, Chicago, 60611, IL, USA.

²Robert H. Lurie Comprehensive Cancer Center, Northwestern University Feinberg School of Medicine, 675 N St Clair St, Chicago, 60611, IL, USA.

*Corresponding author(s). E-mail(s): rendong.yang@northwestern.edu;
Contributing authors: yangyang.li@northwestern.edu;

qingxiang.guo@northwestern.edu;

†These authors contributed equally to this work.

Abstract

Single-cell genomic analysis relies on **whole genome amplification (WGA)** to generate sufficient DNA for sequencing, yet this process introduces chimeric artifacts that manifest as false-positive **structural variation (SV)** and compromise downstream analyses. Here we present ChimeraLM, an interpretable **genomic language model (GLM)** that identifies **WGA**-induced chimeric artifacts directly from sequence information. ChimeraLM is trained on matched **WGA** and bulk sequencing from the same sample, using bulk support to label chimeric reads as amplification-induced artifacts or genuine events. To capture long-range dependencies in variable-length reads, the model combines Hyena operators with attention pooling. Evaluated on matched **WGA** and bulk nanopore datasets, ChimeraLM reduced chimeric reads by ~90%, restoring chimeric rates to near-bulk levels, whereas existing methods achieved at most 8% reduction. When applied to **SV** calling, ChimeraLM reduced unsupported calls by 92–93% while retaining 72–92% of bulk-supported variants. ChimeraLM further normalized **SV**-type distributions toward bulk profiles by suppressing the characteristic **inversion (INV)** bias observed in unprocessed **WGA** data. Attention-based

047 interpretation indicates that ChimeraLM concentrates classification evidence at
048 chimeric junctions, demonstrating capacity to learn biologically interpretable
049 features. ChimeraLM provides a general approach for suppressing amplification-
050 induced artifacts, enabling more reliable single-cell **SV** analysis across long-read
051 platforms.

052 **Keywords:** Whole Genome Amplification, Single Cell, Genomic Language Model,
053 Structural Variation

054

055

056

057 **Main**

058

059 Single-cell and low-input genomics have transformed our ability to resolve biological
060 heterogeneity, enabling the discovery of rare cell states and the reconstruction of clonal
061 evolution in cancer and development [1–3]. However, the limited DNA input (on the
062 order of picograms per cell) makes comprehensive genome-wide profiling technically
063 challenging [4, 5]. **Whole genome amplification (WGA)** therefore remains a prerequisite
064 for high-coverage sequencing [6–8], yet it introduces systematic errors that compromise
065 genomic fidelity, particularly for **structural variation (SV)** detection [9–11].

066 A prominent source of error is amplification-induced chimera formation, in which
067 highly processive polymerases, such as phi29 used in **multiple displacement amplification (MDA)**,
068 switch templates and join discontinuous genomic loci into a single
069 molecule [9–13]. This problem is particularly consequential for long-read sequencing,
070 which is otherwise well suited for resolving complex **SVs**. Chimeric reads can constitute
071 a substantial fraction of **WGA** data [9], generating alignment patterns that resemble
072 genuine **translocations (TRAs)** and **inversions (INVs)** [10]. Consequently, **SV** callers
073 that rely on alignment-based signals (e.g., split-read and supplementary alignments)
074 and coverage-derived evidence frequently misinterpret amplification artifacts as true
075 rearrangements, inflating false positives and distorting **SV** spectra [14–22].

076 Distinguishing genuine genomic rearrangements from amplification artifacts
077 remains a major computational challenge. Existing quality-control approaches typi-
078 cally rely on handcrafted rules or alignment-derived features, such as read orientation
079 signatures or local coverage deviations [11, 13, 23]. However, these heuristics are often
080 sensitive to platform- and protocol-specific variation. Moreover, they cannot capture
081 sequence-level patterns or long-range dependencies within reads. As a result, low-
082 input long-read sequencing remains difficult to deploy in settings where high precision
083 is essential, including somatic mosaicism profiling [24] and validation of CRISPR
084 off-target effects [25].

085 To address this challenge, we present ChimeraLM, an interpretable **genomic lan-**
086 **guage model (GLM)** for identifying and filtering **WGA**-induced artifacts at the
087 single-read level. Unlike traditional approaches that rely on handcrafted rules derived
088 from read alignments or sequence-level [11, 13, 23], ChimeraLM formulates artifact
089 detection as a sequence-modeling task and learns discriminative features directly from
090 raw reads [26]. Building on advances in DNA foundation models [27–30], it captures
091 latent motifs and structural dependencies that generalize across **Oxford Nanopore**
092

Technologies (ONT) platforms. On ONT WGA datasets, ChimeraLM reduces chimeric reads by ~90% while preserving 72–92% of bulk-supported SVs, improving SV validation rates by 8.5- to 11.0-fold and restoring bulk-like SV-type distributions. Together, ChimeraLM provides an effective and interpretable filter for WGA long-read data, enabling robust SV discovery in single-cell and low-input genomics. 093
094
095
096
097
098

Results 099 100

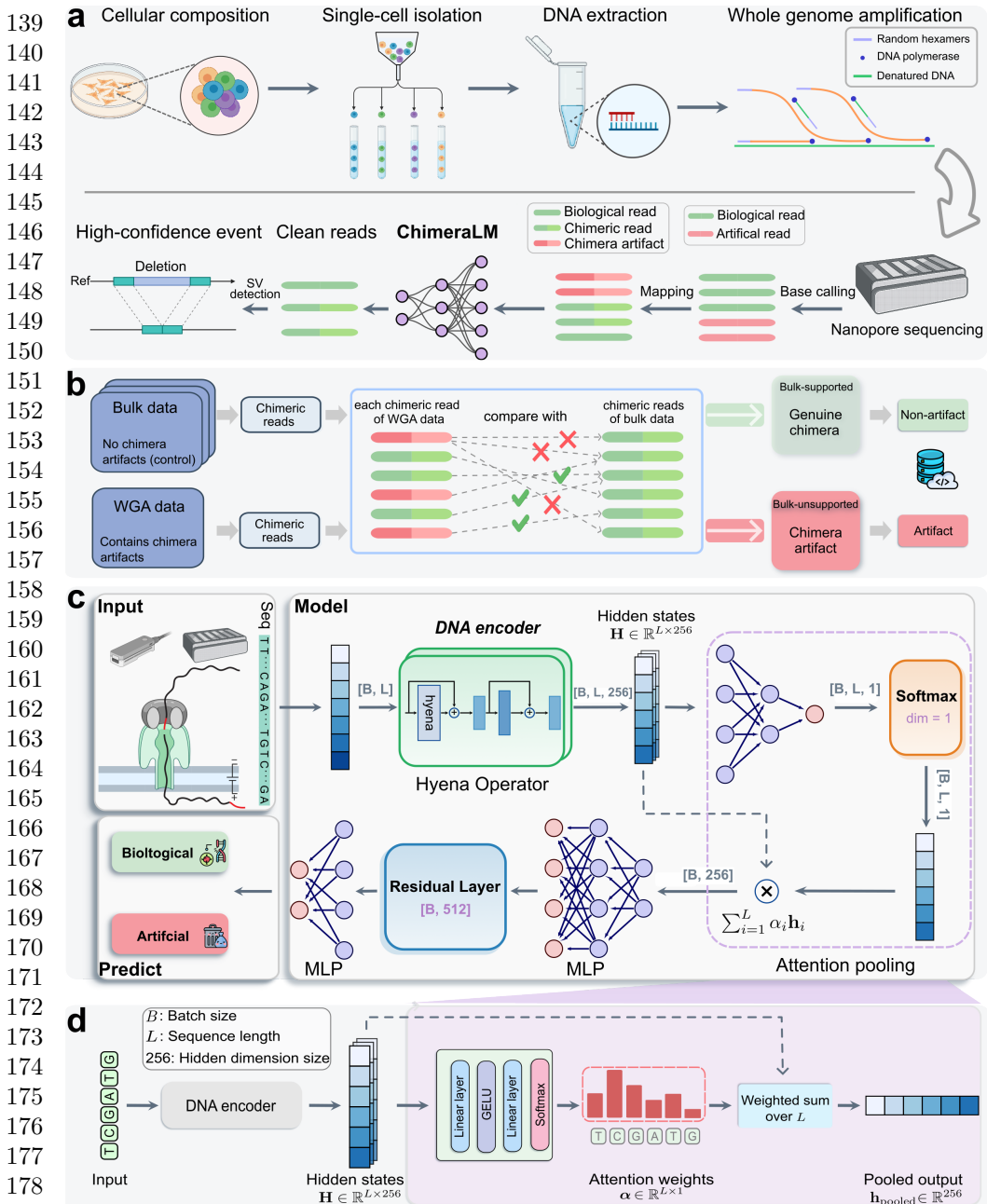
Overview of ChimeraLM workflow and model architecture 101

ChimeraLM integrates into the single-cell long-read workflow as a post-alignment filtering module (Fig. 1a). After base calling and mapping, WGA data contain both genuine chimeric reads and WGA-induced chimeric artifacts. ChimeraLM evaluates reads with chimeric alignments prior to variant calling and classifies each as reflecting a genuine genomic event or an WGA-induced artifact. This binary classification enables selective removal of artificial reads while retaining genuine chimeric events for downstream SV analysis. 102
103
104
105
106
107
108
109

To build a supervised training set we generated WGA long-read sequencing data from PC3 cells on the ONT PromethION platform and collected three matched bulk long-read datasets from unamplified genomic DNA (ONT PromethION, ONT MinION, and Pacific Biosciences (PacBio)). We used the WGA PromethION dataset to construct bulk-supported labels by matching each WGA chimeric read to chimeric alignment structures observed in the bulk references (Methods; Fig. 1b; Extended Data Fig. 1a): reads with bulk-supported alignment structures were labeled as genuine events, whereas reads with no bulk match were labeled as WGA-induced artifacts. To evaluate cross-platform generalization, we generated an independent WGA dataset on the MinION platform, which was reserved exclusively for testing (Extended Data Fig. 1a). 110
111
112
113
114
115
116
117
118
119
120
121
122
123
124
125
126
127
128
129
130
131
132
133
134
135
136
137
138

This labeling procedure classified 12,963,576 chimeric reads from the WGA PromethION dataset into two groups (genuine events and WGA-induced artifacts) based on bulk support (Extended Data Fig. 1b). Among these, 12,670,396 reads (97.7%) showed no matching alignment structures in any bulk dataset and were labeled as WGA-induced artifacts. The remaining 293,180 reads (2.3%) had matching structures in at least one bulk dataset, indicating they represent genuine genomic events rather than amplification artifacts, and were labeled as genuine chimeric reads. To construct a balanced training dataset, we retained all 293,180 genuine chimeric reads and randomly subsampled an equal number of WGA-induced artifacts. We further added 178,748 chimeric reads sampled from the bulk datasets to the genuine-event set, expanding the diversity of bulk-supported chimeric alignment structures used for training. The final labeled dataset comprised 765,108 reads and was split into training (70%), validation (20%), and test (10%) sets using stratified sampling (Extended Data Fig. 1a).

To model these labeled reads, ChimeraLM must process long, variable-length DNA sequences at single-nucleotide resolution (Fig. 1c). We therefore built ChimeraLM on HyenaDNA [27], a genomic foundation model pre-trained on diverse DNA sequences. Each read is tokenized at nucleotide resolution and encoded by Hyena operators [31], which capture long-range sequence context without splitting the input. The encoder 133
134
135
136
137
138



181 Fig. 1 ChimeraLM workflow and architecture for detecting WGA artifacts. (a) Single-cell

182 genomic workflow and ChimeraLM integration. Single cells are isolated, followed by DNA extrac-

183 tion and WGA. During amplification, WGA-induced chimeric artifacts (red) are generated along-

184 side genuine chimeric reads (green). After base calling and mapping, ChimeraLM classifies reads with

185 chimeric alignments as genuine events or WGA-induced artifacts, enabling downstream SV detec-

186 tion on filtered data. (b) Bulk-supported label generation. Chimeric reads from WGA data are com-

187 pared against bulk sequencing from the same cell line. Reads with bulk-supported alignment struc-

188 tures are labeled as genuine events (green); reads with no bulk match are labeled as WGA-induced

189 artifacts (red). (c) ChimeraLM architecture. Input DNA sequences (batch size B , sequence length L)

190 are tokenized at single-nucleotide resolution and encoded into hidden states $H \in \mathbb{R}^{L \times 256}$ through

191 DNA encoder (HyenaDNA [27]). Hyena operators capture long-range dependencies. Attention pool-

192 ing aggregates position-specific features, and multilayer perceptron (MLP) layers with residual connec-

193 tions process pooled representations for binary classification of genuine events and WGA-induced

194 artifacts. (d) Attention pooling mechanism. Attention weights $\alpha \in \mathbb{R}^{L \times 1}$ are computed through linear

195 layers with GELU activation and softmax normalization, assigning importance scores to each

196 position. The weighted sum produces a fixed-dimensional representation $h_{\text{pooled}} \in \mathbb{R}^{256}$. Created

197 with BioRender.com.

produces a sequence of hidden states across the full read. To obtain a fixed-length representation for classification, ChimeraLM uses an attention-pooling module that learns position-specific weights and computes a weighted sum over the hidden states (Fig. 1d). The pooled representation is then passed through residual MLP blocks, and a final softmax outputs the probability that a read reflects a genuine event versus a WGA-induced artifact.

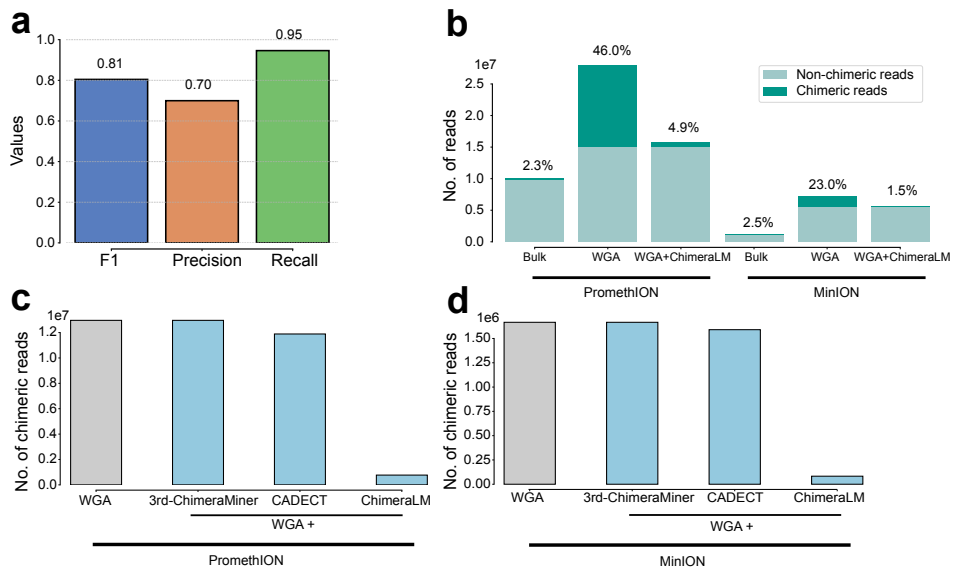


Fig. 2 ChimeraLM accurately identifies and removes WGA-induced chimeric artifacts. (a) Classification performance on held-out test data. ChimeraLM achieves recall of 0.95, precision of 0.70, and F1 score of 0.81. (b) Chimeric read reduction across sequencing platforms. Stacked bars show proportions of chimeric (dark teal) and non-chimeric (light teal) reads in bulk, WGA, and ChimeraLM-filtered samples. ChimeraLM reduces chimeric read frequencies from 46.0% to 4.9% (PromethION) and from 23.0% to 1.5% (MinION), approaching bulk levels (2.3% and 2.5%, respectively). (c,d) Benchmarking against existing methods on PromethION (c) and MinION (d). The gray bar indicates the total number of chimeric read on unfiltered WGA data. The blue bar represents the total number of chimeric reads remaining after filtering by each method. ChimeraLM achieves approximately 90% reduction in chimeric reads on both platforms, while 3rd-ChimeraMiner shows no detectable reduction and CADECT shows 8.3% and 4.6% reduction on PromethION and MinION, respectively. SACRA failed to complete due to memory exhaustion (> 500 GB RAM required).

ChimeraLM achieves high accuracy and reduces artifacts to near-bulk levels across platforms

We first evaluated ChimeraLM on the held-out test set derived from the labeled dataset (Fig. 2a; see Methods). This test set comprises chimeric reads with known biological or artificial status based on the ground-truth labeling procedure described above. On this benchmark, ChimeraLM achieved an F1 score of 0.81, with a recall of 0.95 and a precision of 0.70. The high recall indicates that 95% of artificial chimeric reads were

231 correctly identified and removed, which is critical for minimizing downstream false-
232 positive **SV** calls, while the precision confirms that most flagged reads correspond to
233 true artifacts rather than biological rearrangements.

234 We next asked whether ChimeraLM filtering could restore chimeric read rates in
235 full PC3 **WGA** datasets to bulk baselines on both PromethION and MinION plat-
236 forms (Fig. 2b). Bulk sequencing established low baseline chimeric read rates of 2.3%
237 (PromethION) and 2.5% (MinION). In contrast, **WGA** increased the chimeric frac-
238 tion to 46.0% and 23.0%, respectively. After ChimeraLM filtering, chimeric content
239 dropped to 4.9% on PromethION and 1.5% on MinION, corresponding to 10- to 15-fold
240 reductions, while retaining 15.8 million and 5.6 million biological reads. These post-
241 filtering rates approach bulk baselines, indicating effective removal of **WGA**-induced
242 artifacts while preserving authentic biological signal.

243 We benchmarked ChimeraLM against SACRA [23], 3rd-ChimeraMiner [13], and
244 CADECT [11], existing tools for detecting amplification-induced chimeras (Fig. 2c,d).
245 ChimeraLM achieved approximately 90% reduction in chimeric reads on both plat-
246 forms, substantially outperforming CADECT (8.3% and 4.6% reduction on Prome-
247 thION and MinION, respectively), while 3rd-ChimeraMiner showed no detectable
248 reduction. SACRA could not be evaluated due to out-of-memory errors even with 500
249 GB RAM.

250 The MinION results are particularly informative because this platform was never
251 used during model training. ChimeraLM was trained exclusively on PromethION
252 **WGA** data, yet achieved comparable chimeric read reduction on MinION. This cross-
253 platform generalization indicates that ChimeraLM captures sequence-level features
254 intrinsic to **WGA**-induced artifacts rather than platform-specific signatures, sup-
255 porting its potential applicability to additional long-read and short-read sequencing
256 technologies.

257

258

259

260

261

262

263

264

265

266

267

268

269

270

271

272

273

274

275

276

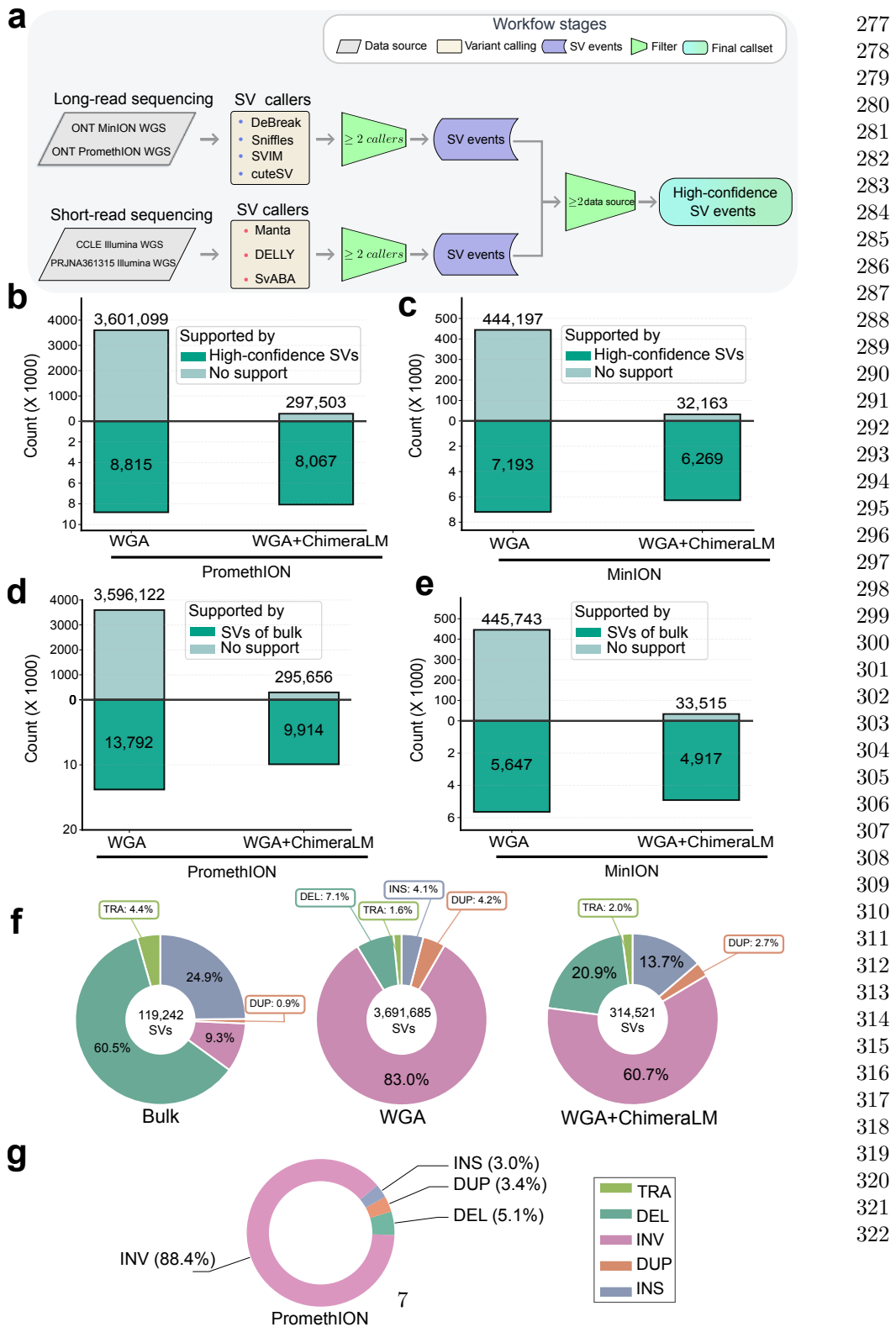


Fig. 3 ChimeraLM improves structural variant detection accuracy. (a) Construction of a high-confidence SV reference dataset from bulk PC3 sequencing. Four bulk datasets were integrated: ONT MinION Mk1C, ONT PromethION P2, the CCLE Illumina whole genome sequencing (WGS) dataset, and the PRJNA361315 Illumina WGS dataset. SVs were called independently within each dataset using multiple callers, and events supported by ≥2 callers per dataset were retained. SVs were then compared across datasets, and events observed in ≥2 of the four bulk datasets were designated as gold-standard SVs. (b,c) SV validation against the gold-standard reference for PromethION (b) and MinION (c). Bars show SV calls supported by the gold standard (dark teal) or unsupported (light teal). (d,e) SV validation against platform-matched long-read bulk sequencing for PromethION (d) and MinION (e), capturing true long-read SVs that may not be represented in the multi-platform reference. Bars show SV calls supported by the platform-matched long-read bulk data (dark teal) or unsupported (light teal). f SV type distributions for PromethION across bulk, unfiltered WGA, and WGA+ChimeraLM. Unfiltered WGA shows an excess of INVs, which is reduced after ChimeraLM filtering. g Composition of artifact-supported SVs for PromethION. Donut charts summarize SV types among events supported exclusively by chimeric reads, representing artificial SVs preferentially removed by ChimeraLM.

323 **ChimeraLM substantially reduces unsupported structural
324 variant calls**

325 Accurate **SV** detection from single cells is essential for understanding genomic diver-
326 sity and disease mechanisms. However, **WGA**-induced chimeric artifacts can be
327 misidentified as genuine **SVs**, leading to incorrect biological conclusions. To quantify
328 ChimeraLM’s impact on **SV** calling, we compared **SV** callsets generated from unfiltered
329 **WGA** reads with those generated after ChimeraLM filtering (**WGA** + ChimeraLM).
330 We evaluated both callsets against two complementary references (Fig. 3): (i) a
331 stringent gold-standard **SV** set derived from bulk PC3 DNA by cross-dataset con-
332 sensus (Fig. 3a), and (ii) platform-matched long-read bulk **SV** callsets used as a
333 platform-specific reference for recall (Fig. 3d,e).

334 We first constructed a high-confidence gold-standard **SV** set from bulk PC3 DNA
335 using four independent sequencing datasets: **ONT** PromethION, **ONT** MinION, and
336 two Illumina whole-genome datasets (the CCLE PC3 **WGS** dataset and PRJNA361315
337 PC3 **WGS** dataset) (Fig. 3a; Extended Data Table 1). **SVs** were called separately
338 within each dataset using multiple **SV** callers. Events supported by at least two callers
339 within a dataset were retained, and only **SVs** observed in at least two of the four
340 datasets were kept as gold-standard events.

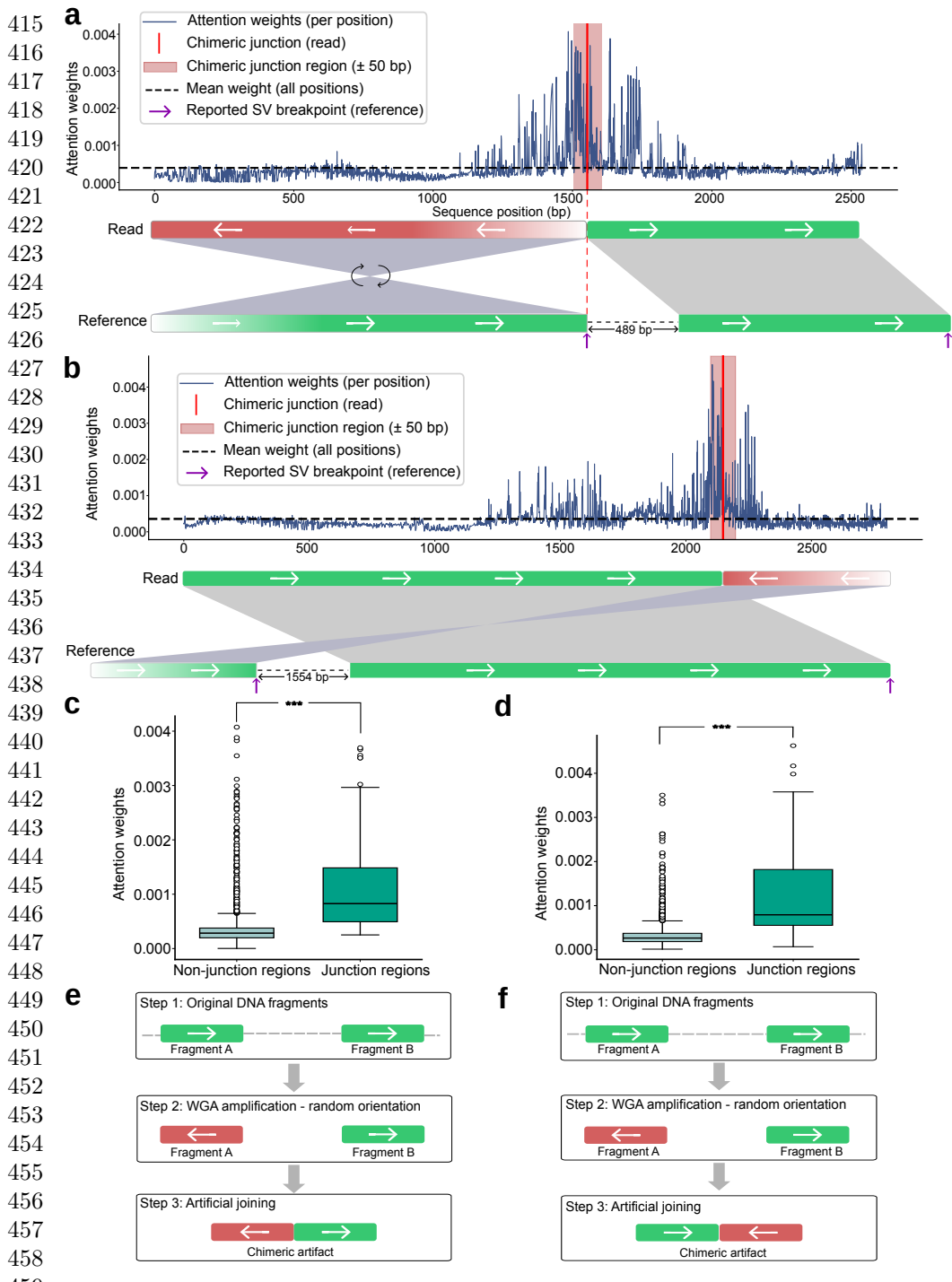
341 Relative to this stringent gold standard, unfiltered **WGA** produced extensive
342 unsupported **SVs** (Fig. 3b,c). On PromethION, **WGA** yielded 3,601,099 **SV** calls, of
343 which only 8,815 (0.24%) overlapped gold-standard events. After ChimeraLM filtering,
344 total calls dropped to 305,570 (91.5% reduction) while retaining 8,067 gold-standard
345 events (91.5% retention), increasing the validation rate to 2.64% (11-fold) (Fig. 3b).
346 On MinION, calls decreased from 451,390 to 38,432 (91.5% reduction), while gold-
347 standard-supported events decreased from 7,193 to 6,269, corresponding to 87.2%
348 retention. The validation rate increased from 1.59% to 16.3% (10-fold) (Fig. 3c).

349 Because the gold standard is intentionally stringent and may miss true **SVs**
350 detectable only in long-read data, we next performed platform-matched validation
351 using long-read bulk sequencing from the same platform (Fig. 3d,e). This analysis pro-
352 vides a platform-specific estimate of recall and reduces bias introduced by the strict
353 gold-standard definition. ChimeraLM increased validation rates from 0.38% to 3.24%
354 on PromethION (8.5-fold) and from 1.25% to 12.79% on MinION (10-fold), while
355 retaining 71.9% and 87.1% of bulk-supported events, respectively. Together, these
356 results show that ChimeraLM removes an order of magnitude of unsupported **SV** calls
357 while preserving the majority of bulk-supported variants across platforms.

359 **360 ChimeraLM restores bulk-like SV-type distributions**

361 Amplification artifacts can distort the apparent spectrum of **SVs**. We therefore com-
362 pared **SV** type distributions across bulk, unfiltered **WGA**, and ChimeraLM-filtered
363 datasets on both nanopore platforms (Fig. 3f; Extend Data Fig. 2). Bulk sequenc-
364 ing showed a balanced mixture of **deletions (DELs)**, **duplications (DUPs)**, **insertions**
365 (**INSs**), **INVs**, and **TRAs**. In contrast, unfiltered **WGA** callsets were dominated by
366 **INVs** on both platforms. After ChimeraLM filtering, excessive **INVs** were markedly

reduced, and the overall SV type profile shifted toward the bulk distribution, while the relative proportions of other SV classes remained largely stable.	369 370
To identify which SV types were primarily driven by WGA -induced artifacts, we examined SV calls supported exclusively by reads classified as chimera artifacts (Fig. 3g; Extend Data Fig. 3). These artifact-supported events were overwhelmingly INVs , accounting for 88.4% on PromethION and 92.4% on MinION. The remaining calls included smaller fractions of DELs (5.1% and 3.8%), DUPs (3.4% and 2.4%), and INSs (3.0% and 1.4%), indicating that WGA -induced chimeras can generate false positives across multiple SV categories.	371 372 373 374 375 376 377
Together, these results show that WGA artifacts preferentially inflate INVs but are not limited to a single SV class. By selectively removing artifact-supported events and restoring SV type distributions toward bulk-like patterns, ChimeraLM improves the robustness and interpretability of single-cell SV analyses.	378 379 380 381 382 383 384 385 386 387 388 389 390 391 392 393 394 395 396 397 398 399 400 401 402 403 404 405 406 407 408 409 410 411 412 413 414



460 **Fig. 4 ChimeraLM attention weights are enriched at chimeric junction regions.**

(a,b) Attention weight profiles for two representative chimeric reads exhibiting distinct junction configurations. Upper panels show per-position attention weights (blue) with the mean attention across the read indicated by a dashed line. Red vertical lines mark inferred chimeric junction positions, and pink shading denotes the junction-centered region (± 50 bp). Lower panels display read-level alignments, highlighting orientation transitions at the junctions (green, forward orientation; red, reverse-complemented orientation). (c,d) Quantitative comparison of attention weights between junction and non-junction regions. Junction-centered windows show significantly elevated attention weights relative to non-junction regions ($P = 5.3 \times 10^{-14}$ and $P = 6.8 \times 10^{-15}$; Wilcoxon rank-sum test). (e,f) Schematic illustration of WGA-induced chimera formation. During amplification, DNA fragments originating from distant genomic loci can be amplified in either orientation, joining them into a single molecule with discordant orientations, producing INV-like alignment signatures. The two examples illustrate forward-to-reverse and reverse-to-forward orientation transitions.

Attention visualization reveals interpretable classification features	461
	462
	463
	464
	465
	466
	467
	468
	469
	470
	471
	472
	473
	474
	475
	476
	477
	478
	479
	480
	481
	482
	483
	484
	485
	486
	487
	488
	489
	490
	491
	492
	493
	494
	495
	496
	497
	498
	499
	500
	501
	502
	503
	504
	505
	506
WGA enables genomic analysis from single cells but introduces chimeric artifacts that compromise SV detection. ChimeraLM addresses this challenge by classifying chimeric reads as biological or artificial from sequence information and filtering WGA -induced artifacts before variant calling, rather than attempting to correct artifact-driven calls post hoc. Across nanopore platforms, ChimeraLM yielded consistent improvements at both read and variant levels. It reduced chimeric reads by ~90% while retaining 72–92% of bulk-supported SVs , and it increased supported SV calls by 8.5–11.0 fold. Performance generalized from PromethION (used for training) to MinION without platform-specific retraining, indicating that ChimeraLM captures properties shared by WGA -induced artifacts rather than instrument-specific signatures.	496
In contrast, existing methods showed limited effectiveness on our ONT WGA datasets. SACRA and 3rd-ChimeraMiner, designed for PacBio platforms [13, 23], either failed to complete (SACRA, >500 GB RAM) or showed no detectable reduction (3rd-ChimeraMiner), highlighting poor cross-platform generalization. CADECT [11] achieved only 8.3% and 4.6% reduction on PromethION and MinION, respectively, despite being developed for Nanopore data. CADECT uses sliding-window self-alignment to detect concatemers, which are reads containing tandem duplications with internal sequence similarity. This fundamental design limitation explains CADECT’s modest performance. These results demonstrate that heuristics targeting specific artifact subtypes cannot comprehensively address the diversity of amplification-induced	497

507 chimeras and highlight the need for learning-based models that capture discriminative
508 sequence patterns without relying on predefined structural assumptions.

509 The efficacy of ChimeraLM highlights the utility of deep learning in quality control
510 tasks where conventional metrics (e.g., mapping quality, read depth) provide limited
511 resolution [11, 13, 23, 26]. By learning directly from sequence data, ChimeraLM discov-
512 ers subtle compositional and structural features that differentiate authentic sequences
513 from amplification artifacts. The model also offers interpretability through attention
514 visualization: attention weights concentrate at junction regions where template switch-
515 ing joins discordant loci, validating the biological relevance of the learned features.
516 These methodological advances have direct implications for single-cell genomics, where
517 high false-positive rates in **WGA** data have constrained robust characterization of
518 chromosomal instability, clonal evolution, and **SV** burden [20, 22, 32]. By improving
519 the signal-to-noise ratio and clarifying **SV**-type spectra that are otherwise distorted
520 by amplification artifacts, ChimeraLM enables more confident identification of gen-
521 uine **SVs**, supporting studies of cancer evolution, developmental biology, and somatic
522 mosaicism where single-cell resolution is essential [24, 25].

523 Several limitations warrant consideration. First, the current model processes reads
524 independently; integrating contextual features such as coverage or phasing informa-
525 tion may further enhance accuracy. Second, regarding computational resources, while
526 **central processing unit (CPU)** inference is feasible, **graphics processing unit (GPU)**
527 acceleration is recommended for processing large-scale datasets. Finally, future work
528 should extend validation to diverse cell types, sequencing platforms (e.g., PacBio HiFi),
529 and alternative **WGA** protocols—including **multiple annealing and looping-based**
530 **amplification cycles (MALBAC)** [33], **linear amplification via transposon insertion**
531 (**LIANTI**) [5], **primary template-directed amplification (PTA)** [19], and **droplet-based**
532 **MDA (dMDA)** [34]. Although the sequence-level approach implies effective trans-
533 ferability, such broad validation is essential to optimize performance across specific
534 amplification chemistries.

535 Broadly, ChimeraLM illustrates the potential of **GLMs** for genomic data quality
536 control. With emerging long-context architectures [27], the model’s context window
537 could be extended to 1M tokens, enabling analysis of increasingly complex genomic
538 structures. This framework could extend to other amplification-dependent technolo-
539 gies, such as cell-free DNA analysis, ancient DNA studies, and metagenomics from
540 low-biomass samples. Furthermore, attention-based interpretability opens opportuni-
541 ties for studying template-switching dynamics, potentially guiding the development of
542 improved amplification protocols. In summary, ChimeraLM provides a practical and
543 interpretable framework for enhancing long-read single-cell genomic fidelity, ensuring
544 that downstream biological insights are derived from genuine **SVs** rather than technical
545 artifacts.

546

547

548

549

550

551

552

Methods	553
Cell culture, single-clone preparation, and nanopore sequencing	554
<i>Cell culture and single-clone establishment</i>	555
PC3 prostate cancer cells (ATCC® CRL-1435™) were cultured in RPMI-1640 medium supplemented with 10% fetal bovine serum and 1% penicillin–streptomycin at 37 °C with 5% CO ₂ . To minimize biological heterogeneity, a monoclonal population was established by serial dilution in 96-well plates, ensuring that each culture originated from a single cell. Mycoplasma contamination was routinely tested and confirmed negative prior to DNA extraction.	556
<i>DNA extraction and whole-genome amplification</i>	557
From the monoclonal population, two types of DNA samples were prepared: a bulk (non-amplified) control and ten single-cell MDA-amplified genomes. Bulk high-molecular-weight DNA was extracted using the Monarch® HMW DNA Extraction Kit for Cells & Blood (New England Biolabs). Individual cells were isolated using 1CellDish-60 mm (iBiochips) and amplified using the REPLI-g Advanced DNA Single Cell Kit (Qiagen) following the manufacturer's protocol. DNA concentration and fragment integrity were assessed with a Qubit 4 fluorometer and Agilent TapeStation (DNA 1000/5000 ScreenTape). Only samples meeting quality standards were used for library construction.	558
<i>Nanopore library preparation and sequencing</i>	559
Libraries were prepared using the ONT Ligation Sequencing Kit V14 (SQK-LSK114) and sequenced on MinION Mk1C or PromethION P2 Solo devices with R10.4.1 flow cells following the manufacturer's genomic DNA workflow. Because all single-cell samples originated from the same monoclonal lineage, differences between amplified and bulk datasets primarily reflect MDA-induced artifacts rather than biological variation.	560
<i>Basecalling and read processing</i>	561
POD5 files were basecalled using Dorado v0.5.0 with the high-accuracy model dna_r10.4.1_e8.2_400bps_hac@v4.3.0 [35]. Reads with mean quality < 10 or length < 500 bp were removed. Adapters and concatemers were trimmed using Cutadapt v4.0 [36] in a two-pass, error-tolerant procedure. Filtered reads were aligned to the GRCh38.p13 reference genome using minimap2 v2.26 (map-ont preset) [37]. BAM files were sorted and indexed using SAMtools v1.16 [38]. Read-length and mapping statistics were computed using NanoPlot v1.46.1 [39]. All samples were processed using identical parameters.	562
<i>Chimeric read identification</i>	563
Chimeric reads were identified from BAM files using supplementary alignment (SA) tags. Reads were classified as chimeric if they (i) were mapped, (ii) contained an SA tag, (iii) were primary alignments (not secondary), and (iv) were not supplementary alignments themselves. This definition counts each chimeric read once using its primary	564
	565
	566
	567
	568
	569
	570
	571
	572
	573
	574
	575
	576
	577
	578
	579
	580
	581
	582
	583
	584
	585
	586
	587
	588
	589
	590
	591
	592
	593
	594
	595
	596
	597
	598

599 alignment while excluding secondary/supplementary records, thereby avoiding double-
600 counting and reducing ambiguity from low-confidence alignments. Reads lacking **SA**
601 tags were classified as non-chimeric.

602

603 **Training data construction**

604

605 *Data generation and sources*

606 To construct the training dataset, we generated **WGA** and bulk sequencing data from
607 PC3 cells. The **WGA** sample was amplified and sequenced on the PromethION P2 plat-
608 form (**ONT**), while three independent bulk datasets were produced from non-amplified
609 genomic DNA: bulk PromethION P2, bulk MinION Mk1c (**ONT**), and bulk **PacBio**.
610 These bulk datasets represent authentic biological sequences free from amplification-
611 induced artifacts. In contrast, **WGA** sequencing includes both genuine genomic reads
612 and artificial chimeras introduced during the amplification process.

613

614 *Ground truth annotation and class definition*

615 Ground truth labels were established by systematically comparing chimeric reads from
616 the **WGA** PromethION P2 dataset against those from the three bulk datasets. For each
617 **WGA** chimeric read, all alignment segments—defined by their genomic start and end
618 coordinates—were compared to the corresponding segments of bulk chimeric reads.
619 A **WGA** read was labeled as biological if every segment matched at least one bulk
620 chimeric read within a 1 kb positional tolerance, indicating that the structural con-
621 figuration is also present in non-amplified DNA. Reads lacking any matching pattern
622 across all bulk datasets were labeled as artificial chimeras, presumed to arise from the
623 amplification process. Additional chimeric reads were randomly sampled from the bulk
624 datasets and labeled as biological, as these reads originate from genuine genomic rear-
625 rangements such as true **SVs**. The final labeled dataset combined the annotated **WGA**
626 PromethION P2 reads with the subsampled bulk chimeric reads and was subsequently
627 partitioned into training, validation, and test sets as described below.

628

629 *Dataset partitioning and cross-platform validation*

630 The combined labeled dataset, derived from **WGA** PromethION P2 and bulk sequenc-
631 ing data, was divided into training (70%), validation (20%), and test (10%) sets using
632 stratified random sampling. These subsets were used respectively for model training,
633 hyperparameter tuning, and performance evaluation on data from the same sequencing
634 platform.

635

636 To evaluate cross-platform generalization, the complete **WGA** MinION Mk1c
637 dataset was reserved. This dataset, generated on a different nanopore platform,
638 was never used during model training or internal testing. This two-level evaluation
639 design allowed us to test whether ChimeraLM captures general sequence features of
640 amplification-induced chimeras rather than platform-specific artifacts.

641

642

643

644

Model architecture	645
DNA encoder	646

ChimeraLM employs the pre-trained HyenaDNA model [27] as its DNA encoder. This model was pre-trained on large-scale genomic data and provides robust sequence representations. DNA sequences are tokenized at single-nucleotide resolution, with each base (A, C, G, T, N) mapped to a unique integer token (7, 8, 9, 10, 11, respectively). Special tokens include [CLS]=0, [PAD]=4, and others for sequence processing. Input sequences are truncated at 32,768 bp or padded to enable batch processing.

For a tokenized input sequence $\mathbf{x} \in \mathbb{Z}^L$, the HyenaDNA generates contextualized hidden representations:

$$\mathbf{H} = \text{HyenaDNA}(\mathbf{x}) \in \mathbb{R}^{L \times 256}$$

where $\mathbf{H} = (\mathbf{h}_1, \mathbf{h}_2, \dots, \mathbf{h}_L)$ represents position-wise hidden states with dimension 256. The Hyena operators [31] efficiently capture both local sequence motifs and long-range dependencies essential for distinguishing biological sequences from chimeric artifacts.

Attention pooling

To aggregate variable-length sequence representations into fixed-size vectors, ChimeraLM implements attention-based pooling. For hidden states $\mathbf{H} \in \mathbb{R}^{L \times 256}$, attention weights are computed through a two-layer network:

$$\begin{aligned} \mathbf{e} &= \text{GELU}(\text{Linear}_{256 \rightarrow 256}(\mathbf{H})) \in \mathbb{R}^{L \times 256} \\ \mathbf{s} &= \text{Linear}_{256 \rightarrow 1}(\mathbf{e}) \in \mathbb{R}^{L \times 1} \\ \boldsymbol{\alpha} &= \text{softmax}(\mathbf{s}) \in \mathbb{R}^{L \times 1} \end{aligned}$$

The pooled representation is the weighted sum of hidden states:

$$\mathbf{h}_{\text{pooled}} = \sum_{i=1}^L \alpha_i \mathbf{h}_i \in \mathbb{R}^{256}$$

This mechanism assigns learned importance weights to each sequence position, enabling the model to focus on informative regions while accommodating natural variability in read lengths.

Classification head

The pooled representation is processed through a MLP with residual connections. The first layer expands dimensionality:

$$\mathbf{f}_1 = \text{Dropout}_{0.1}(\text{GELU}(\text{Linear}_{256 \rightarrow 512}(\mathbf{h}_{\text{pooled}}))) \in \mathbb{R}^{512}$$

Subsequent residual blocks with input $\mathbf{f}_{\text{in}} \in \mathbb{R}^{512}$ compute:

$$\mathbf{f}_{\text{out}} = \text{Dropout}_{0.1}(\text{Linear}_{512 \rightarrow 512}(\text{GELU}(\text{Linear}_{512 \rightarrow 512}(\mathbf{f}_{\text{in}})))) + \mathbf{f}_{\text{in}}$$

691 where the skip connection enables stable gradient flow during training. The final layer
692 produces binary classification logits:

693

694 $\mathbf{z} = [z_0, z_1] = \text{Linear}_{512 \rightarrow 2}(\mathbf{f}_{\text{final}}) \in \mathbb{R}^2$

695

696 where z_0 and z_1 represent logits for biological and artificial chimeric classes, respec-
697 tively. During inference, the predicted class is $\hat{y} = \text{argmax}_{i \in \{0,1\}} z_i$.

698

699 ***Model summary***

700 The complete ChimeraLM pipeline processes DNA sequences through: (1) single-
701 nucleotide tokenization, (2) HyenaDNA backbone encoding to generate contextualized
702 representations, (3) attention pooling to aggregate position-specific features, (4)
703 **MLP** layers with residual connections to learn classification features, and (5) binary
704 classification output. The entire model is trained end-to-end using labeled data.

705

706 **Model training and optimization**

707

708 ***Training configuration***

709 ChimeraLM was trained using PyTorch [40] and PyTorch Lightning [41] frameworks.
710 Input sequences were tokenized using the tokenizer with maximum sequence length of
711 32,768 bp. Sequences longer than this threshold were truncated; shorter sequences were
712 padded to enable batch processing. Training employed mixed-precision computation
713 (bf16) to accelerate training while maintaining numerical stability.

714

715 ***Optimization procedure***

716 We used the AdamW optimizer [42] with learning rate $\eta = 1 \times 10^{-4}$ and weight
717 decay $\lambda = 0.01$. AdamW implements adaptive learning rates with decoupled weight
718 decay, combining the benefits of Adam optimization with proper L2 regularization.
719 A ReduceLROnPlateau scheduler dynamically adjusted the learning rate based on
720 validation loss, reducing it by a factor of 0.1 when no improvement occurred for 10
721 consecutive epochs. Early stopping with patience of 10 epochs prevented overfitting
722 by terminating training when validation performance plateaued. A fixed random seed
723 (12345) ensured reproducibility across training runs.

724 The training objective used cross-entropy loss for binary classification. For a
725 training example with class label $y \in \{0, 1\}$ and model logits $\mathbf{z} = [z_0, z_1]$, the loss is:
726

727

$$728 \mathcal{L}(\mathbf{z}, y) = -\log \left(\frac{\exp(z_y)}{\exp(z_0) + \exp(z_1)} \right) = -z_y + \log(\exp(z_0) + \exp(z_1))$$

729

730 where z_0 and z_1 represent logits for biological and artificial chimeric classes, respec-
731 tively.

732

733 ***Training implementation***

734

735 Training used batch size of 16 sequences with 30 parallel data loading workers. **GPU**
736 acceleration was employed for efficient processing, with training typically requiring

55 hours. Model checkpointing saved the best-performing model based on validation metrics. Configuration management used Hydra [43] to enable reproducible experimentation.

Model evaluation

Performance was monitored using precision, recall, and F1 score on the validation set after each epoch:

$$\text{Precision} = \frac{\text{TP}}{\text{TP} + \text{FP}}, \quad \text{Recall} = \frac{\text{TP}}{\text{TP} + \text{FN}}$$
$$\text{F1} = \frac{2 \times \text{Precision} \times \text{Recall}}{\text{Precision} + \text{Recall}}$$

where TP (true positives) are chimeric reads correctly classified as artificial, TN (true negatives) are biological reads correctly classified as biological, FP (false positives) are biological reads misclassified as artificial, and FN (false negatives) are artificial reads misclassified as biological. Final model selection was based on best validation performance as determined by early stopping.

Model inference and application

Inference pipeline

To apply ChimeraLM to new WGA sequencing data, the model takes a BAM file as input. Chimeric reads are identified using SA tags and filtered to exclude unmapped, secondary, or supplementary alignments. Each chimeric read sequence is tokenized using the tokenizer (maximum length 32,768 bp, with truncation or padding as needed). The trained model processes sequences in batches, generating two logits $[z_0, z_1]$ for each read corresponding to biological and artificial chimeric classes. Classification is determined by $\hat{y} = \text{argmax}(z_0, z_1)$. ChimeraLM outputs a filtered BAM file containing only reads classified as biological, which can be directly used for downstream analyses including SV calling.

Performance evaluation

Test set evaluation

Final model performance was evaluated on the held-out test set and the independent MinION Mk1c dataset. Metrics (precision, recall, and F1 score) were computed as described in the training section, where true positives represent chimeric reads correctly classified as artificial and true negatives represent biological reads correctly classified as biological.

SV calling

SVs were called using multiple tools to ensure comprehensive detection. For long-read data (ONT PromethION P2 and MinION Mk1c), we used Sniffles v2.5 [14, 15], DeBreak v1.2 [16], SVIM v2.0.0 [17], and cuteSV v2.1.1 [18]. For short-read data of the PC3 cell line, we used both the CCLE Illumina WGS dataset and the PRJNA361315

783 Illumina **WGS** dataset, processed with Manta v1.6.0 [44], DELLY v1.5.0 [45], and
784 SvABA v1.1.0 [46]. All tools were executed with default recommended parameters.

785

786 ***Gold standard SV dataset construction***

787 To evaluate the impact of ChimeraLM on **SV** detection accuracy, we generated a high-
788 confidence gold-standard **SV** set from bulk PC3 sequencing data. All **SV** comparisons
789 and breakpoint corrections were performed using OctopuSV v0.2.3 [47]. Four bulk
790 datasets were integrated: **ONT** MinION Mk1c, **ONT** PromethION P2, the CCLE Illumina
791 **WGS** dataset, and the PRJNA361315 Illumina **WGS** dataset. **SVs** were called
792 independently within each dataset, and events supported by at least two **SV** callers
793 were retained. The remaining calls were then compared across datasets, and **SVs**
794 observed in at least two of the four datasets were designated as gold-standard events
795 for benchmarking.

796

797 ***SV benchmarking analysis***

798 To assess the impact of ChimeraLM on **SV** calling accuracy, we compared **SV** calls from
799 unfiltered **WGA** data and ChimeraLM-filtered **WGA** data against two references: (1)
800 the stringent multi-platform gold standard dataset, and (2) platform-matched long-
801 read bulk sequencing data. Benchmarking was performed using Truvari v4.2.2 [48]
802 with default parameters. **SVs** were considered supported if they matched reference
803 variants within the defined breakpoint tolerance. Validation rates were calculated as
804 the proportion of called **SVs** supported by the reference. This dual benchmarking
805 strategy quantifies both improvements in detecting high-confidence multi-platform
806 **SVs** and the retention of platform-specific true variants.

807

808 **Benchmarking against existing methods**

809 ChimeraLM was compared to existing computational methods for detecting
810 amplification-induced chimeric artifacts: SACRA [23] (GitHub commit 9a2607e), 3rd-
811 ChimeraMiner [13] (GitHub commit 04b5233), and CADECT v1.2 [11]. Both tools
812 were applied to **WGA** data from PromethION P2 and MinION Mk1c platforms using
813 default parameters as recommended in their documentation. Performance was eval-
814 uated by measuring the percentage reduction in chimeric reads relative to unprocessed
815 **WGA** data. Chimeric reads were identified using **WGA** tag-based alignment criteria
816 (reads with **SA** tags indicating split alignments), and reduction rates were calculated
817 as the proportion of chimeric reads removed by each method.

818

819 **Attention weight analysis**

820

821 To investigate ChimeraLM's interpretability, we analyzed attention weights from
822 the pooling mechanism for representative chimeric reads. Attention weights indicate
823 the relative importance assigned to each sequence position during classification. For
824 selected reads, we extracted per-position attention weights and visualized them along-
825 side read alignments to identify whether the model focuses on mechanistically relevant
826 regions.

827

828

Chimeric junction positions were identified from alignment data (defined by break-points in SA tags). A region of ± 50 bp surrounding each junction was designated as the junction region. Attention weights within junction region were compared to non-junction regions using the Wilcoxon rank-sum test [49], with statistical significance assessed at $p < 0.001$. 829
830
831
832
833
834

Data visualization

Figures were generated using Python with Matplotlib [50] and Seaborn [51]. 835
836
837

Computing resources

Computations were performed on a high performance computing (HPC) server with 64-core Intel Xeon Gold 6338 CPU, 256 GB RAM, and two NVIDIA A100 GPUs (80 GB memory each). 838
839
840
841
842
843
844
845

Extended Data Table 1 Sequencing and alignment statistics of PC3

Sample	Platform	Reads ($\times 10^6$)	Total bases (Gb)	Total bases aligned (Gb)	Fraction aligned	Mean length (bp)	Mean quality (Q)	Average identity (%)
WGA	MinION	9.11	14.6	10.4	0.7	1,603	14.3	97.6
WGA	PromethION	44.69	128.2	69.2	0.5	2,869	14.5	96.1
Bulk	MinION	0.97	8.1	7.1	0.9	8,310	17.2	97.3
Bulk	PromethION	8.00	69.9	62.4	0.9	8,732	18.5	97.7

Supplementary information.

875

876

877

878

879

880

881

882

883

884

885

886

887

888

889

890

891

Extended Data Fig. 1 Training dataset construction and bulk-supported labeling strategy. (a) Workflow for generating labeled training data. **WGA** PromethION data is compared against three independent bulk sequencing datasets (PromethION, MinION, and PacBio). Reads with no bulk matches (Match 0) are labeled artificial; reads matching one or more bulk datasets (Match 1–3) are labeled biological, along with chimeric reads sampled directly from bulk data. The labeled dataset is split into training (70%), validation (20%), and test (10%) sets. The **WGA** MinION dataset is reserved for independent cross-platform evaluation. (b) Distribution of chimeric read matches. Bar chart shows the number of **WGA** PromethION chimeric reads (log scale) by bulk dataset matches. Match 0 reads ($\sim 10^7$) lacking bulk validation are classified as artificial; Match 1–3 reads with bulk support are classified as biological. The substantial imbalance reflects high prevalence of **WGA**-induced artifacts.

901

902

903

904

905

906

907

908

909

910

911

912

913

914

915

Extended Data Fig. 2 SV type distributions for MinION across bulk, unfiltered WGA, and WGA+ChimeraLM. Unfiltered **WGA** shows an excess of **INVs**, which is reduced after ChimeraLM filtering.

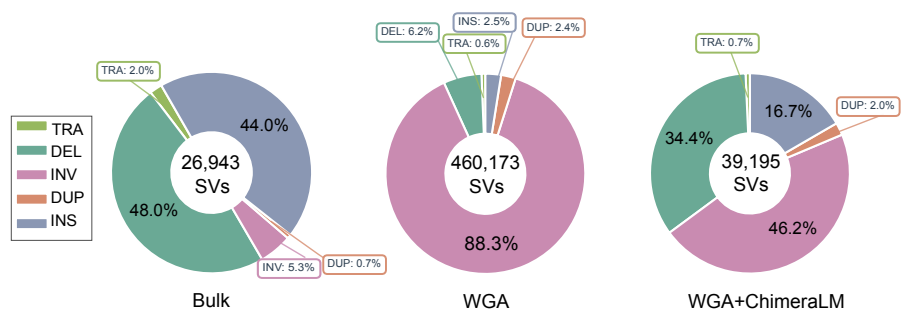
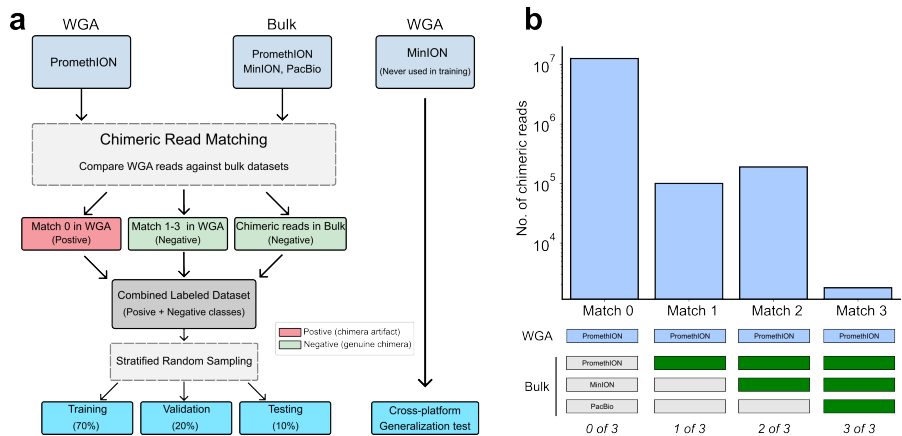
916

917

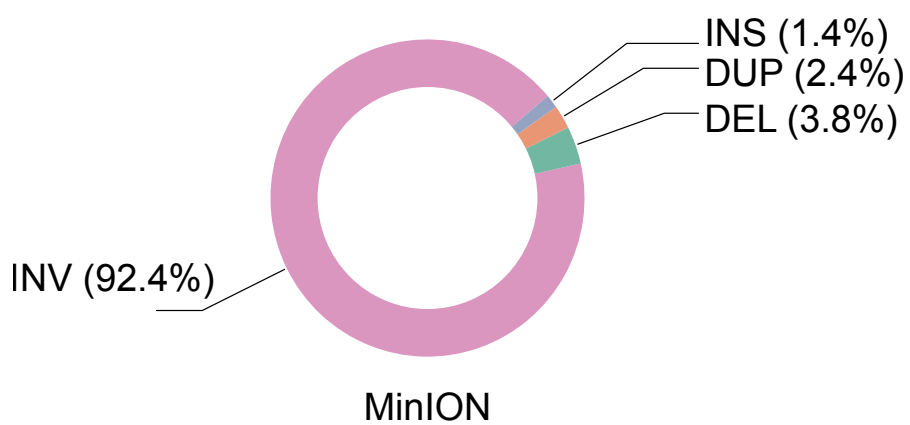
918

919

920



921
922
923
924
925
926
927
928
929
930
931
932
933
934
935
936
937
938
939
940
941
942
943
944
945
946
947
948
949
950
951
952
953
954
955
956
957
958
959
960
961
962
963
964
965
966



Extended Data Fig. 3 Composition of artifact-supported **SVs for MinION.** Donut charts summarize **SV** types among events supported exclusively by chimeric reads, representing artificial **SVs** preferentially removed by ChimeraLM.

967 **Acknowledgements.** We thank Tingyou Wang for guidance on figure preparation.
968 This project was supported in part by NIH grants R35GM142441 and R01CA259388
969 awarded to RY.

970

971 **Declarations**

972

973 **Author Contributions.** YL, QG and RY designed the study. YL and QG per-
974 formed the analysis. QG performed the experiments. YL and QG designed and
975 implemented the model. YL built the command-line tool and documentation. YL, QG
976 and RY wrote the manuscript. RY supervised this work.

977

978 **Data Availability.** The raw sequencing data generated in this study have been
979 deposited in the NCBI Sequence Read Archive (SRA) under BioProject accession
980 PRJNA1354861. The dataset includes Oxford Nanopore long-read whole-genome
981 sequencing of PC3 prostate cancer cells and MDA-amplified single-cell derivatives. The
982 individual SRA accessions are as follows: PC3 bulk (MinION Mk1C), SRR35904028;
983 PC3 bulk (PromethION P2), SRR35904029; PC3 10-cell WGA (MinION Mk1C),
984 SRR35904026; PC3 10-cell WGA (PromethION P2), SRR35904027. We can access the
985 data at the following link: [https://dataview.ncbi.nlm.nih.gov/object/PRJNA1354861?
986 reviewer=viej6cv6mgbli3n7a9a5k1bsb3](https://dataview.ncbi.nlm.nih.gov/object/PRJNA1354861?reviewer=viej6cv6mgbli3n7a9a5k1bsb3)

986

987 **Code Availability.** ChimeraLM, implemented in Python, is open source and
988 available on GitHub (<https://github.com/ylab-hi/ChimeraLM>) under the Apache
989 License, Version 2.0. The package can be installed via PyPI ([https://pypi.org/project/
990 chimeralm](https://pypi.org/project/chimeralm)) using pip, with wheel distributions provided for Windows, Linux, and
991 macOS to ensure easy cross-platform installation. An interactive demo is available on
992 Hugging Face (<https://huggingface.co/spaces/yangliz5/ChimeraLM>), allowing users
993 to test DeepChopper's functionality without local installation. For large-scale anal-
994 yses, we recommend using ChimeraLM on systems with **GPU** acceleration. Detailed
995 system requirements and optimization guidelines are available in the repository's
996 documentation (<https://ylab-hi.github.io/ChimeraLM/>).

997

998 **Conflict of interest.** RY has served as an advisor/consultant for Tempus AI, Inc.
999 This relationship is unrelated to and did not influence the research presented in this
1000 study.

1001

1002 **Acronyms**

1003

1004 **CPU** central processing unit [12](#)

1005 **DEL** deletion [8, 9](#)

1006 **dMDA** droplet-based MDA [12](#)

1007 **DUP** duplication [8, 9](#)

1008

1009 **GLM** genomic language model [1, 2, 12](#)

1010 **GPU** graphics processing unit [12, 16, 19, 22](#)

1011

1012 **HPC** high performance computing [19](#)

INS insertion	8, 9	1013
INV inversion	1, 2, 7–10, 20	1014
		1015
LIANTI linear amplification via transposon insertion	12	1016
		1017
MALBAC multiple annealing and looping-based amplification cycles	12	1018
MDA multiple displacement amplification	2	1019
MLP multilayer perceptron	4, 5, 15, 16	1020
ONT Oxford Nanopore Technologies	2, 3, 7, 8, 11, 13, 14, 17, 18	1021
		1022
PacBio Pacific Biosciences	3, 14	1023
PTA primary template-directed amplification	12	1024
		1025
SA supplementary alignment	13, 14, 17–19	1026
SV structural variation	1–4, 6–9, 11, 12, 14, 17, 18, 20, 21	1027
		1028
TRA translocation	2, 8	1029
		1030
WGA whole genome amplification	1–12, 14, 17–20	1031
WGS whole genome sequencing	7, 8, 17, 18	1032
		1033
		1034
		1035
		1036
		1037
		1038
		1039
		1040
		1041
		1042
		1043
		1044
		1045
		1046
		1047
		1048
		1049
		1050
		1051
		1052
		1053
		1054
		1055
		1056
		1057
		1058

References

- [1] Kalef-Ezra, E. *et al.* Single-cell somatic copy number variants in brain using different amplification methods and reference genomes. *Communications Biology* 1288 (2024).
- [2] Navin, N. *et al.* Tumour evolution inferred by single-cell sequencing. *Nature* **472**, 90–94 (2011).
- [3] Sun, C. *et al.* Mapping recurrent mosaic copy number variation in human neurons. *Nature Communications* 4220 (2024).
- [4] Gawad, C., Koh, W. & Quake, S. R. Single-cell genome sequencing: current state of the science. *Nature Reviews Genetics* 175–188 (2016).
- [5] Chen, C. *et al.* Single-cell whole-genome analyses by linear amplification via transposon insertion (LIANTI). *Science (new York, N.Y.)* **356**, 189–194 (2017).
- [6] Macaulay, I. C. & Voet, T. Single cell genomics: Advances and future perspectives. *PLOS Genetics* **10**, e1004126 (2014).
- [7] de Bourcy, C. F. A. *et al.* A quantitative comparison of single-cell whole genome amplification methods. *PLoS ONE* e105585 (2014).
- [8] Biezuner, T. *et al.* Comparison of seven single cell whole genome amplification commercial kits using targeted sequencing. *Scientific Reports* 17171 (2021).

- 1059 [9] Lu, N., Qiao, Y., Lu, Z. & Tu, J. Chimera: The spoiler in multiple displacement
1060 amplification. *Computational and Structural Biotechnology Journal* 1688–1696
1061 (2023).
- 1062
- 1063 [10] Lasken, R. S. & Stockwell, T. B. Mechanism of chimera formation during the
1064 multiple displacement amplification reaction. *BMC Biotechnology* **7**, 19 (2007).
- 1065
- 1066 [11] Agyabeng-Dadzie, F. *et al.* Evaluating the benefits and limits of multiple displace-
1067 ment amplification with whole-genome oxford nanopore sequencing. *Molecular*
1068 *Ecology Resources* e14094 (2025).
- 1069
- 1070 [12] Dean, F. B. *et al.* Comprehensive human genome amplification using multiple
1071 displacement amplification. *Proceedings of the National Academy of Sciences* **99**,
1072 5261–5266 (2002).
- 1073
- 1074 [13] Lu, N. *et al.* Exploration of whole genome amplification generated chimeric
1075 sequences in long-read sequencing data. *Briefings in Bioinformatics* **24**, bbad275
1076 (2023).
- 1077
- 1078 [14] Sedlazeck, F. J. *et al.* Accurate detection of complex structural variations using
1079 single-molecule sequencing. *Nature Methods* 461–468 (2018).
- 1080
- 1081 [15] Smolka, M. *et al.* Detection of mosaic and population-level structural variants
1082 with sniffles2. *Nature Biotechnology* 1571–1580 (2024).
- 1083
- 1084 [16] Chen, Y. *et al.* Deciphering the exact breakpoints of structural variations using
1085 long sequencing reads with DeBreak. *Nature Communications* 283 (2023).
- 1086
- 1087 [17] Heller, D. & Vingron, M. SVIM: Structural variant identification using mapped
1088 long reads. *Bioinformatics* 2907–2915 (2019).
- 1089
- 1090 [18] Jiang, T. *et al.* Long-read-based human genomic structural variation detection
1091 with cuteSV. *Genome Biology* 189 (2020).
- 1092
- 1093 [19] Gonzalez-Pena, V. *et al.* Accurate genomic variant detection in single cells with
1094 primary template-directed amplification. *Proceedings of the National Academy of*
1095 *Sciences* **118**, e2024176118 (2021).
- 1096
- 1097 [20] Kosugi, S. *et al.* Comprehensive evaluation of structural variation detection
1098 algorithms for whole genome sequencing. *Genome Biology* **20**, 117 (2019).
- 1099
- 1100 [21] Alkan, C., Coe, B. P. & Eichler, E. E. Genome structural variation discovery and
1101 genotyping. *Nature Reviews Genetics* **12**, 363–376 (2011).
- 1102
- 1103 [22] Hård, J. *et al.* Long-read whole-genome analysis of human single cells. *Nature*
1104 *Communications* **14**, 5164 (2023).

- [23] Kiguchi, Y., Nishijima, S., Kumar, N., Hattori, M. & Suda, W. Long-read metagenomics of multiple displacement amplified DNA of low-biomass human gut phageomes by SACRA pre-processing chimeric reads. *DNA Research* **28**, dsab019 (2021).
1105
1106
1107
1108
1109
1110
1111
1112
1113
1114
1115
1116
1117
1118
1119
1120
1121
1122
1123
1124
1125
1126
1127
1128
1129
1130
1131
1132
1133
1134
1135
1136
1137
1138
1139
1140
1141
1142
1143
1144
1145
1146
1147
1148
1149
1150
- [24] Ha, Y.-J. *et al.* Comprehensive benchmarking and guidelines of mosaic variant calling strategies. *Nature Methods* **20**, 2058–2067 (2023).
1105
1106
1107
1108
1109
1110
1111
1112
1113
1114
1115
1116
1117
1118
1119
1120
1121
1122
1123
1124
1125
1126
1127
1128
1129
1130
1131
1132
1133
1134
1135
1136
1137
1138
1139
1140
1141
1142
1143
1144
1145
1146
1147
1148
1149
1150
- [25] Höijer, I. *et al.* Amplification-free long-read sequencing reveals unforeseen CRISPR-Cas9 off-target activity. *Genome Biology* **21**, 290 (2020).
1105
1106
1107
1108
1109
1110
1111
1112
1113
1114
1115
1116
1117
1118
1119
1120
1121
1122
1123
1124
1125
1126
1127
1128
1129
1130
1131
1132
1133
1134
1135
1136
1137
1138
1139
1140
1141
1142
1143
1144
1145
1146
1147
1148
1149
1150
- [26] Li, Y. *et al.* A genomic language model for chimera artifact detection in nanopore direct rna sequencing. *bioRxiv* (2024). URL <https://www.biorxiv.org/content/early/2024/10/25/2024.10.23.619929>.
1105
1106
1107
1108
1109
1110
1111
1112
1113
1114
1115
1116
1117
1118
1119
1120
1121
1122
1123
1124
1125
1126
1127
1128
1129
1130
1131
1132
1133
1134
1135
1136
1137
1138
1139
1140
1141
1142
1143
1144
1145
1146
1147
1148
1149
1150
- [27] Nguyen, E. *et al.* *HyenaDNA: Long-range genomic sequence modeling at single nucleotide resolution*, Vol. 36, 43177–43201 (Curran Associates, Inc., 2023).
1105
1106
1107
1108
1109
1110
1111
1112
1113
1114
1115
1116
1117
1118
1119
1120
1121
1122
1123
1124
1125
1126
1127
1128
1129
1130
1131
1132
1133
1134
1135
1136
1137
1138
1139
1140
1141
1142
1143
1144
1145
1146
1147
1148
1149
1150
- [28] Dalla-Torre, H. *et al.* Nucleotide transformer: building and evaluating robust foundation models for human genomics. *Nature Methods* 287–297 (2025).
1105
1106
1107
1108
1109
1110
1111
1112
1113
1114
1115
1116
1117
1118
1119
1120
1121
1122
1123
1124
1125
1126
1127
1128
1129
1130
1131
1132
1133
1134
1135
1136
1137
1138
1139
1140
1141
1142
1143
1144
1145
1146
1147
1148
1149
1150
- [29] Zhou, Z. *et al.* *DNABERT-2: Efficient foundation model and benchmark for multi-species genomes*, 1–24 (OpenReview.net, 2024).
1105
1106
1107
1108
1109
1110
1111
1112
1113
1114
1115
1116
1117
1118
1119
1120
1121
1122
1123
1124
1125
1126
1127
1128
1129
1130
1131
1132
1133
1134
1135
1136
1137
1138
1139
1140
1141
1142
1143
1144
1145
1146
1147
1148
1149
1150
- [30] Consens, M. E. *et al.* To transformers and beyond: Large language models for the genome (2023). [arXiv:2311.07621](https://arxiv.org/abs/2311.07621).
1105
1106
1107
1108
1109
1110
1111
1112
1113
1114
1115
1116
1117
1118
1119
1120
1121
1122
1123
1124
1125
1126
1127
1128
1129
1130
1131
1132
1133
1134
1135
1136
1137
1138
1139
1140
1141
1142
1143
1144
1145
1146
1147
1148
1149
1150
- [31] Poli, M. *et al.* *Hyena hierarchy: Towards larger convolutional language models*, Vol. 202, 28043–28078 (PMLR, 2023).
1105
1106
1107
1108
1109
1110
1111
1112
1113
1114
1115
1116
1117
1118
1119
1120
1121
1122
1123
1124
1125
1126
1127
1128
1129
1130
1131
1132
1133
1134
1135
1136
1137
1138
1139
1140
1141
1142
1143
1144
1145
1146
1147
1148
1149
1150
- [32] Mahmoud, M. *et al.* Structural variant calling: The long and the short of it. *Genome Biology* **20**, 246 (2019).
1105
1106
1107
1108
1109
1110
1111
1112
1113
1114
1115
1116
1117
1118
1119
1120
1121
1122
1123
1124
1125
1126
1127
1128
1129
1130
1131
1132
1133
1134
1135
1136
1137
1138
1139
1140
1141
1142
1143
1144
1145
1146
1147
1148
1149
1150
- [33] Zong, C., Lu, S., Chapman, A. R. & Xie, X. S. Genome-wide detection of single-nucleotide and copy-number variations of a single human cell. *Science* 1622–1626 (2012).
1105
1106
1107
1108
1109
1110
1111
1112
1113
1114
1115
1116
1117
1118
1119
1120
1121
1122
1123
1124
1125
1126
1127
1128
1129
1130
1131
1132
1133
1134
1135
1136
1137
1138
1139
1140
1141
1142
1143
1144
1145
1146
1147
1148
1149
1150
- [34] Dippenaar, A. *et al.* Droplet based whole genome amplification for sequencing minute amounts of purified mycobacterium tuberculosis DNA. *Scientific Reports* **14**, 9931 (2024).
1105
1106
1107
1108
1109
1110
1111
1112
1113
1114
1115
1116
1117
1118
1119
1120
1121
1122
1123
1124
1125
1126
1127
1128
1129
1130
1131
1132
1133
1134
1135
1136
1137
1138
1139
1140
1141
1142
1143
1144
1145
1146
1147
1148
1149
1150
- [35] PLC., O. N. Dorado. <https://github.com/nanoporetech/dorado> (2023).
1105
1106
1107
1108
1109
1110
1111
1112
1113
1114
1115
1116
1117
1118
1119
1120
1121
1122
1123
1124
1125
1126
1127
1128
1129
1130
1131
1132
1133
1134
1135
1136
1137
1138
1139
1140
1141
1142
1143
1144
1145
1146
1147
1148
1149
1150
- [36] Martin, M. Cutadapt removes adapter sequences from high-throughput sequencing reads. *Embo Journal* **17**, 10–12 (2011).
1105
1106
1107
1108
1109
1110
1111
1112
1113
1114
1115
1116
1117
1118
1119
1120
1121
1122
1123
1124
1125
1126
1127
1128
1129
1130
1131
1132
1133
1134
1135
1136
1137
1138
1139
1140
1141
1142
1143
1144
1145
1146
1147
1148
1149
1150
- [37] Li, H. Minimap2: Pairwise alignment for nucleotide sequences. *Bioinformatics* 3094–3100 (2018).
1105
1106
1107
1108
1109
1110
1111
1112
1113
1114
1115
1116
1117
1118
1119
1120
1121
1122
1123
1124
1125
1126
1127
1128
1129
1130
1131
1132
1133
1134
1135
1136
1137
1138
1139
1140
1141
1142
1143
1144
1145
1146
1147
1148
1149
1150

- 1151 [38] Danecek, P. *et al.* Twelve years of SAMtools and BCFtools. *GigaScience* giab008
1152 (2021).
- 1153
- 1154 [39] De Coster, W. & Rademakers, R. NanoPack2: Population-scale evaluation of
1155 long-read sequencing data. *Bioinformatics* **39**, btad311 (2023).
- 1156
- 1157 [40] Paszke, A. *et al.* *PyTorch: An imperative style, high-performance deep learning
library*, Vol. 32, 8024–8035 (Curran Associates, Inc., 2019).
- 1158
- 1159 [41] Falcon, W. & The PyTorch Lightning team. PyTorch Lightning. GitHub
1160 repository (2019). URL <https://github.com/Lightning-AI/lightning>.
- 1161
- 1162 [42] Loshchilov, I. & Hutter, F. *Decoupled weight decay regularization* (2019).
- 1163
- 1164 [43] Yadan, O. Hydra - a framework for elegantly configuring complex applications.
1165 GitHub repository (2019). URL <https://github.com/facebookresearch/hydra>.
- 1166
- 1167 [44] Chen, X. *et al.* Manta: Rapid detection of structural variants and indels for
1168 germline and cancer sequencing applications. *Bioinformatics* 1220–1222 (2016).
- 1169
- 1170 [45] Rausch, T. *et al.* DELLY: Structural variant discovery by integrated paired-end
1171 and split-read analysis. *Bioinformatics* i333–i339 (2012).
- 1172
- 1173 [46] Wala, J. A. *et al.* SvABA: Genome-wide detection of structural variants and
1174 indels by local assembly. *Genome Research* 581–591 (2018).
- 1175
- 1176 [47] Guo, Q., Li, Y., Wang, T.-Y., Ramakrishnan, A. & Yang, R. OctopusV and
1177 TentacleSV: A one-stop toolkit for multi-sample, cross-platform structural variant
1178 comparison and analysis. *Bioinformatics* btaf599 (2025).
- 1179
- 1180 [48] English, A. C., Menon, V. K., Gibbs, R. A., Metcalf, G. A. & Sedlazeck, F. J.
1181 Truvari: Refined structural variant comparison preserves allelic diversity. *Genome
Biology* **23**, 271 (2022).
- 1182
- 1183 [49] Virtanen, P. *et al.* SciPy 1.0: Fundamental algorithms for scientific computing in
1184 python. *Nature Methods* 261–272 (2020).
- 1185
- 1186 [50] Hunter, J. D. Matplotlib: A 2d graphics environment. *Computing in Science &
1187 Engineering* 90–95 (2007).
- 1188
- 1189 [51] Waskom, M. L. seaborn: statistical data visualization. *Journal of Open Source
1190 Software* 3021 (2021).
- 1191
- 1192
- 1193
- 1194
- 1195
- 1196